

Evaluation of the Antiviral Potential of Halogenated Dihydrorugosaflavonoids and Molecular Modeling with nsP3 Protein of Chikungunya Virus (CHIKV)

Ninad V. Puranik,^{†,§,||} Ruchi Rani,^{‡,||} Vedita Anand Singh,[‡] Shailly Tomar,^{*,‡}
Hemalata M. Puntambekar,^{†,§} and Pratibha Srivastava^{*,†,§,||}

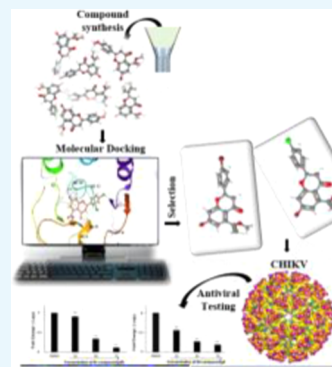
[†]Bioprospecting Group, Agharkar Research Institute, G. G. Agarkar Road, Pune 411004, Maharashtra, India

[‡]Department of Biotechnology, Indian Institute of Technology Roorkee, Roorkee, Uttarakhand 247667, India

[§]Savitribai Phule Pune University, Ganeshkhind, Pune 411007, India

Supporting Information

ABSTRACT: Antiviral therapy is crucial for the circumvention of viral epidemics. The unavailability of a specific antiviral drug against the chikungunya virus (CHIKV) disease has created an alarming situation to identify or develop potent chemical molecules for remedial management of CHIKV. In the present investigation, in silico studies of dihydrorugosaflavonoid derivatives (**5a–f**) with non-structural protein-3 (nsP3) were carried out. nsP3 replication protein has recently been considered as a possible antiviral target in which crucial inhibitors fit into the adenosine-binding pocket of the macrodomain. The 4'-halogenated dihydrorugosaflavonoids displayed intrinsic binding with the nsP3 macrodomain (PDB ID: 3GPO) of CHIKV. Compounds **5c** and **5d** showed docking scores of -7.54 and -6.86 kcal mol $^{-1}$, respectively. Various in vitro assays were performed to confirm their (**5a–f**) antiviral potential against CHIKV. The non-cytotoxic dose was determined by 3-(4,5-dimethylthiazol-2-yl)-2,5-diphenyltetrazolium bromide assay and was found to be $<100\ \mu\text{M}$. The compounds **5c** and **5d** showed their inhibitory potential for CHIKV, which was determined through cytopathic effect assay and plaque reduction assay, which show inhibition up to 95 and 92% for 70 μM concentration of the compounds, respectively. The quantitative real-time polymerase chain reaction assay result confirmed the ability of **5c** and **5d** to reduce the viral RNA level at 70 μM concentration of compounds to nearly 95 and 93% concentration, respectively, in cells with CHIKV infection. Further, the CHIKV-inhibitory capacity of these compounds was corroborated by execution of immunofluorescence assay. The executed work will be meaningful for the future research of studied dihydrorugosaflavonoids against prime antiviral entrants, leading to remedial management to preclude CHIKV infection.



INTRODUCTION

The cases of chikungunya viral fever are burgeoning every year. Infections are not only limited to Asia and Africa; recently, the epidemics of chikungunya have been reported from Central and South America.^{1,2} Concerning the data obtained from the National Vector Borne Disease Control Programme (NVBDCP, India), the number of infected people identified in April 2018 was 9175, 4875 from Karnataka following 1375 from Gujarat and 966 from Maharashtra. Earlier research studies have shown that there is considerable resource burden from chikungunya outbreaks, which escalates in monsoon and post-monsoon seasons. Therefore, cases of chikungunya viral fever have increased in the continent of Asia and various parts of the world. The name chikungunya originates from “Makonde”, meaning “to become twisted”. It denotes the “curved” appearance of those going through joint ache as a result of chikungunya infection. Chikungunya virus (CHIKV) spreads by mosquito vectors *Aedes aegypti* and *Aedes albopictus*. The common eukaryotic hosts are primates and humans. In humans, the symptoms associated with CHIKV are nausea, fever, joint pain, vomiting, rashes, and persistent arthralgia.

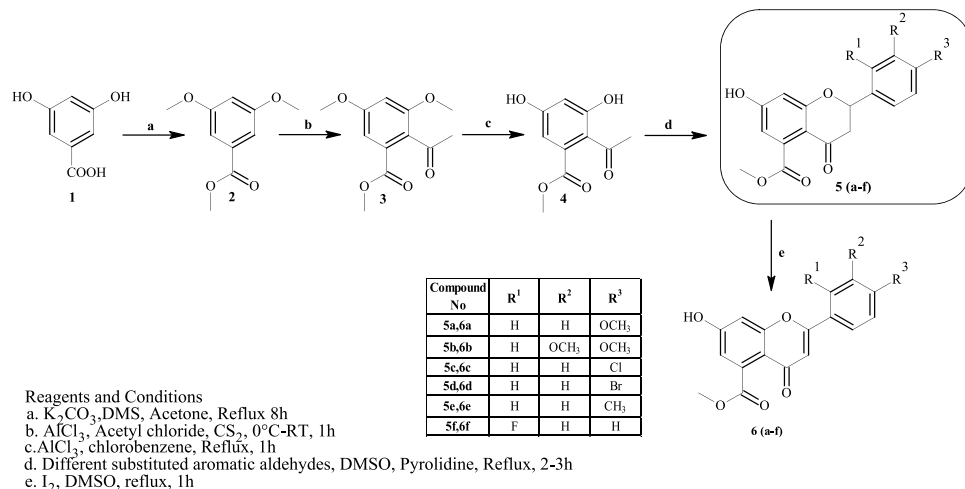
Clinical manifestation is one of the bases for the diagnosis of chikungunya infection, but the confirmation of disease can only be made after laboratory tests. Suspected cases are validated by positive anti-Chikungunya virus IgM or IgG results or by positive polymerase chain reaction (PCR) results.^{3,4}

In Togaviridae family, CHIKV comes under the genus Alphavirus. Alphaviruses are configured as enveloped positive-sense single-stranded RNA viruses. There are 29 members in the alphavirus genus; some members of the genus contain several animal and human viruses like Ross River virus, Sindbis virus (SINV), Western equine encephalitis virus (WEEV), Semiliki Forest virus (SFV), Venezuelan equine encephalitis virus (VEEV), etc. They are furthermore categorized into Old World and New World viruses reliant on the changes that occurred in their life cycle, fatality, and clinical manifestations. Basically, the Old World viruses CHIKV, SINV, SFV, etc.

Received: September 6, 2019

Accepted: November 6, 2019

Published: November 18, 2019

Scheme 1. Schematic Depiction of the Synthesis of Dihydrorugosaflavonoids^{30,31}

engage the protein nsP2 to downregulate the host cell transcription, have less demise percentage, and stimulate arthralgia. The New World viruses VEEV, WEEV, etc. use virus capsid protein (CP) to downregulate the host cell transcription, have high casualty frequency, and generate encephalitis.

Crystallographic studies and cryoelectron microscopy of different alphaviruses and their proteins deliver vital information regarding the molecular organization and the distribution of the virion structural portions.⁵⁻¹² Encapsidated by 240 copies of CP, the RNA genome of CHIKV makes the nucleocapsid core.^{13,14} The grown-up alphavirus virion (70 nm in diameter) has an envelope, which is derived from the host, having $T = 4$ icosahedral symmetry embedded with 80 spikes. Trimers of E1 and E2 (surface glycoproteins) heterodimers build up every spike.¹⁵ CHIKV bears a genome of almost ~11.7 kb, polyadenylated at the 3' end and capped at the 5' end. The non-structural polyproteins (nsP1234) are encoded by the 5' two-third open reading frame (ORF) of the genome. The three chief structural proteins (capsid (C), E1, and E2) are encoded by the 3' one-third ORF of the genome.¹⁶ The functioning of non-structural protein (nsP) promotes the construction of distinct mature non-structural proteins (nsP1–4). nsP1 is the capping enzyme, nsP2 is the viral helicase and protease, and nsP4 is RNA-dependent RNA polymerase, which has an intrinsically disordered N-terminal domain.¹⁷ The role of nsP3 was not very well defined. However, recently, McPherson et al.¹⁸ have reported that CHIKV's nsP3 macrodomain hydrolyzes ADP-ribose groups from mono-(ADP-ribosyl)ated proteins and the activity of nsP3 mono-(ADP-ribosyl)hydrolase is somewhere decisive for CHIKV replication and virulence in mice. At the N-terminus, nsP3 encompasses a very preserved MacroD-type macrodomain. The protein fold in the macrodomain is remarkably conserved, which is present in numerous plus-strand RNA viruses, and it attaches to ADP-ribose. Mutant viruses missing hydrolase activity were incapable of replicating in mammalian BHK-21 cells or mosquito, *A. albopictus*, cells and quickly regressed the catalytically inactivated mutants.

Despite the increasing number of chikungunya patients, haplessly, to date, no antiviral remedy or vaccine is available in the market for the cure of CHIKV-infected patients. Some CHIKV vaccine approaches have been analyzed, together with

inefficient, live weakened, and DNA chimeric vaccines. However, questions associated with protection and efficiency have stalled the development of current vaccine entrants.^{19,20} Besides, drugs testified via in vitro screening of chloroquine, ribavirin, and arbidol to curb CHIKV progress have failed to produce noteworthy therapeutic aids in clinical samples.²¹⁻²⁴ In the recent past, high-throughput assays have been established to figure out probable inhibitors of CHIKV. Literature search has provided the information regarding analysis of 356 natural product molecules and clinically recommended medicines to counteract CHIKV replicon, and an accompanying test with the surrogate infection model of Semliki Forest virus (SFV),²⁵ during analyses of 3040 small compounds as inhibitors of CHIKV nsP2, was also tested by the phenotypic assay protocol.²⁶ Still, the problem for the prevention and treatment of CHIKV fever is recalcitrant. Therefore, it is necessary to work in a streamlined manner to overcome this severe menace.

Flavones are naturally occurring polyphenolic secondary metabolites that exist all over in plants. They have shown enormous potential in the field of medicinal chemistry.²⁷ They are very beneficial in our daily life²⁸ to boost up immunity and can be used as a preventive measure for various ailments, by consuming flavone-rich products such as green tea, fruits, etc. In our laboratory, we had prepared naturally occurring rugosaflavonoid and its derivatives.^{29,30} Before formation of rugosaflavonoids, we had obtained dihydrorugosaflavonoids (Scheme 1).^{30,31} We had screened these compounds for tuberculosis in our previous studies, and we found that halogenated dihydrorugosaflavonoids were much better antitubercular agents than rugosaflavonoids.³¹

Due to nonavailability of the antiviral drug against CHIKV, mostly natural compounds have been subjected to screening for antiviral activity to obtain lead molecules using high-throughput assays.³²⁻³⁵ Therefore, in this study, we have checked the antiviral potential of our compounds against the CHIKV. First, using molecular docking, the target site for the compounds was identified in CHIKV. The non-structural viral proteins have a crucial role in the replication and survival of CHIKV. Among nsP1–nsP4, nsP3 has a natural ligand ADP-ribose that binds to its macrodomain, which is highly conserved.³⁶ The docking of these compounds into the nsP3 macrodomain indicated that the halogenated dihydrorugosa-

flavonoids interacted and fitted more effectively in its pocket. This binding property of halogenated dihydrorugosaflavonoids with nsP3 invigorated us to screen these compounds for antiviral efficacy against CHIKV.

In this study, the docking potential of dihydrorugosaflavonoid derivatives with the macrodomain of nsP3 and their antiviral potential against CHIKV are reported. Based on the outcomes of antiviral screening using CHIKV-infected Vero cells, the dihydrorugosaflavonoids were assessed with several assays. The cytopathic effect (CPE) inhibition and plaque reduction assays were conducted to determine the inhibitory potential of compounds on CHIKV replication, and quantitative real-time polymerase chain reaction (qRT-PCR) was performed to assess the reduction of viral RNA levels in the infected cells. An immunofluorescence assay (IFA) was carried out to investigate the reduction in CHIKV antigen upon treatment with the screened compounds.

■ RESULTS AND DISCUSSION

Chemistry. The dihydrorugosaflavonoid moiety has three rings A, B, and C (Figure 1).^{30,31} All of the synthesized

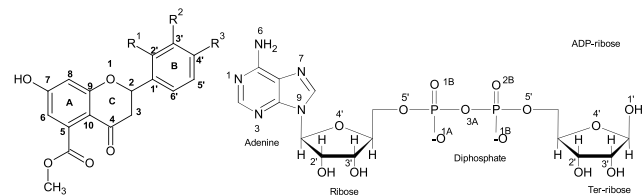


Figure 1. Basic backbone of dihydrorugosaflavonoid and ADP-ribose with numbering. Note: This figure has similarity with that in our previous paper, which has been shown in ref 31. ADP-ribose is a known structure, which has been drawn by us and also shown in ref 47.

compounds have dissimilarities in ring B. The ring A has a hydroxyl group at the 7th position and an ester group at the 5th position. Rest of the changes are only in ring B with differently substituted benzene. They were obtained during the synthesis of analogues of rugosaflavonoid (**6a–f**) as an intermediate before the synthesis of the final product (Scheme 1).³¹

As per Gaspar et al.,²⁷ flavonoids are still a valid scaffold in medicinal chemistry. Recently, Lani et al. have published the antiviral potential of baicalein and fisetin against CHIKV.³⁴ These compounds possessed the same backbone, so it was pertinent to check their inhibitory potential for CHIKV. Recently, the synthesis of these compounds has been reported by our group.³⁰ All of the spectral data have been provided in the Supporting Information (Supporting Information File 1).

In Silico Studies. Molecular Docking of nsP3 with Halogenated Dihydrorugosaflavonoids. The nsP3 has three key domains, a central zinc-binding region, a very conserved N-terminal macrodomain, and a poorly conserved, not properly structured acidic and highly phosphorylated C-terminal domain. The functions of various cellular proteins to influence signaling, stress granule assembly, and viral replication are controlled by the C-terminal domain.^{35,36} The exact role of the central zinc-binding region and N-terminal macrodomain is not well categorized. Macrodomains are known to have a conserved protein fold detected from archaea to higher eukaryotes considered for their affinity to the small molecule ADP-ribose and its analogues. In positive-strand RNA viruses such as alphaviruses, coronaviruses, and hepatitis E virus, the

macrodomains are the integral part of the nsPs.^{37–46} According to Rungrotmongkol et al.,⁴⁷ the molecular understanding of the particular binding of ADP-ribose to the CHIKV nsP3 macrodomain revealed that nsP3 amino acids Asp 10, Ile 11, Asn 24, Asp 31, Gly 32, Val 33, Cys 34, Ser 110–Tyr 114, Val 133, and Arg 144 act as the critical residues in the binding pocket, which make molecular contacts with the ligand. Also, the ribose and diphosphate units of the ADP-ribose were found to play a significant role in making molecular contacts with the amino acid residues of nsP3 in the CHIKV nsP3–ADP-ribose complex (Figure 2a,b).

The chloro derivative of dihydrorugosaflavonoid (**5c**) showed interaction of halogen with Arg 144 (Figure 2c). The carbonyl oxygen of ring C formed hydrogen bonds with Ser 110, Thr 111, and Gly 112. Asp 10 and Ile 11 are also nearby. Val 33 interacted with ring oxygen. **5c** also showed bonding with Leu 109. Thr 114 interacted with the carboxylate group attached with ring A. All of these amino acid residues of the binding pocket are critical and are also active in the binding of nsp3 macrodomain with ADP-ribose (Table 2).

The bromo derivative of rugosaflavonoid (**5d**) showed binding in the potential site pocket of the nsp3 macrodomain and showed interactions with Asn 24, Gly 112, and Asp 31 (Figure 2d). The docking scores of **5c** and **5d** were found to be −7.54 and −6.86 kcal mol^{−1}, respectively (Table 1). These effective binding interactions (Table 2) indicate that these compounds may interfere with the function of nsP3 macrodomain and thus inhibit the replication of CHIKV. Therefore, to evaluate the inhibitory potential of halogenated dihydrorugosaflavonoids against CHIKV, the antiviral assays were performed using Vero cell lines by observing the cytopathic effect (CPE), plaque reduction assay, the quantification of the viral genome RNA by qRT-PCR, and using immunofluorescence imaging.

ADME/T Analysis. In the process of drug discovery development, various rules were considered but suffered various limitations.⁴⁸ Therefore, a combination of pharmacodynamics (PD) and pharmacokinetics (PK), which explains the interaction of an organism with the drug, is important to be studied. PD evaluates what the drug does to the body, and PK explains how body responds to the drug. The main components of PK are absorption, distribution, metabolism, and excretion (ADMET), finally associated with toxicity (ADMET). Although ADMET properties explain the utmost pharmacological performance of small molecules, the toxicology study ensures no injury to the organism with no side effects. According to Hodgson, “A chemical cannot be a drug, no matter how active nor how specific its action, unless it is also taken appropriately into the body (absorption), distributed to the right parts of the body, metabolized in a way that does not instantly remove its activity, and eliminated in a suitable manner—a drug must get in, move about, hang around, and then get out”.⁴⁹ Haplessly, to address all of these parameters is time-consuming and cumbersome due to the intricacy of human body, where all of these parameters affect each other. It has not only limitations to interactions within the body but also several restrictions due to gender, age, genetic state, disease, etc. In this case, in silico technologies can be helpful to compute these calculations based on the mathematical algorithm used in the in silico software. Although it does not give full guaranty that it is going to work 100% in the living system, it saves our time in the selection of molecule

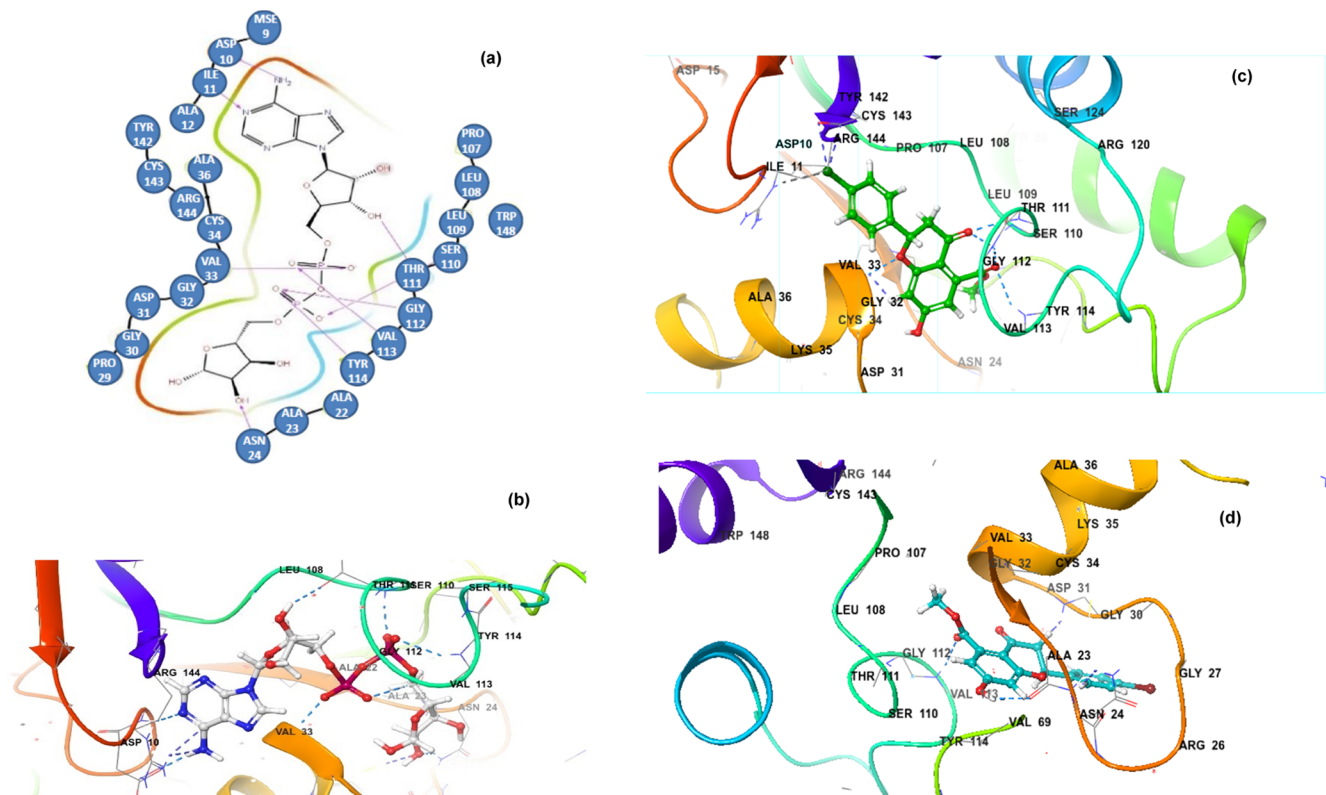


Figure 2. Molecular docking of nsP3 with natural ligand ADP-ribose and dihydrorugosaflavonoids. (a) Two-dimensional image of ligand interaction of nsP3 with ADP-ribose in the binding pocket; (b) three-dimensional ligand interaction diagram of nsP3 with ADP-ribose showing critical residues of nsP3 (binding pocket) such as residues Asp 10, Ile 11, Arg 144 (with adenine), Asn 24, Asp 31–Cys 34 (with sugar moiety), Ser 110–Tyr 114, and Leu 108 (with phosphate group) entailed in interactions with ADP-ribose; (c) interactions of the chloro derivative of dihydrorugosaflavonoid (**5c**) with nsP3, with hydrogen bonds shown in blue and halogen bonds in gray; and (d) interactions of the bromo derivative of dihydrorugosaflavonoid (**5d**) with nsP3.

Table 1. Docking Score and Interacting Residues of 3GPO with **5a–f**

S. No	Structure	Docking Score	Interacting residue
5a		-4.76	Val33, Leu108, Tyr142, Arg144, Asp145
5b		-5.81	Val33, Leu108, Ser110, Tyr142, Arg144, Asp145
5c		-7.54	Val33, Ser110, GLy112, Thr111, Tyr114, Arg144,
5d		-6.86	Asn24, Asp31, Gly112,
5e		-6.12	Val33, Leu108, Tyr142, Arg144, Asp145
5f		-6.55	Val33, Leu108, Tyr142, Arg144, Asp145
std	ADP ribose ⁵²	-9.6/-12.8	Asp10, Ile11, Asn24, Val33, Ser110, Arg144, Tyr114,

to be considered for further studies. Therefore, ADME/T properties were studied using Qikprop software of Maestro.

In Table 3,³¹ values of parameters such as QP log Po/w, QP log HERG, QPP Caco, QP log BB, QPP MDCK, QP log K_p, QP log K_{hsa}, and percentage of human oral

absorption are shown for compounds **5a–f**. QP log Po/w reports the expected octanol/water partition coefficient. Its range should be -2 to 6.5. The values for **5a–f** obtained were between 2.2 and 2.7. QP log HERG predicts IC₅₀ values for the blockage of HERG K⁺ channels. Its defined range is above

Table 2. Interaction Analysis of CHIKV nsP3 with ADP-Ribose and Halogenated Dihydrorugosaflavonoids

s. no.	ADP-ribose	5c	5d
1	H-bond of Asp 10 with N ⁶ of adenine	Asp 10 nearby	Asp 10 nearby
2.	H-bond of Ile 11 with N ¹ of adenine	Ile 11 nearby	Ile 11 nearby
3.	H-bond of O ^{3'} of ribose with Thr 111	Thr 111 interacted with C=O, ring O	Thr 111 is present in cyan near the flavone moiety
4.	interaction of Arg 144 and adenine	interaction of Arg 144 with halogen in ring B	no interaction with Arg 144
5.	O ^{1a} of phosphate with Val 33	ring oxygen in ring C with Val 33	Val 33 showed no interaction
6.	O ^{1b} -O ^{2b} of phosphate with Ser 110	C=O group in ring c with Ser 110	Ser 110 is present in the cyan green loop nearby
7.	O ^{2b} H-bond with Gly 112 and Tyr 114	Gly 112 interacted with C=O in ring C and Tyr 114 interacted with C=O of the carboxylate group	Gly 112 interacted with carbonyl oxygen of the carboxylate group
8.	H-bond of O ^{1'} with Asn 24	no interaction with Asn 24	interaction with Asn 24
9.	no interaction with Asp 31	no interaction with Asp 31	interaction with Asp 31

Table 3. Evaluation of Druglike Properties of the Lead Molecules by the Qikprop Maestro 11.2 Molecular Docking Suite^{a 31}

s. no.	sample ID	QP log Po/ w (-2.0 to 6.5)	QP log HERG (acceptable range: above -5.0)	QPP Caco (nm s ⁻¹) <25, poor >500-great	QP log BB (-3 to 1.2)	QPP MDCK (nm s ⁻¹) <25- poor >500-great	QP log K _p (-8.0 to -0.1)	QP log K _{hsa} (acceptable range: -1.5 to 1.5)	percentage of human oral absorption; (<25% is poor and >80% is high)
1	5a	2.318	-4.879	411.852	-1.037	150.21	-2.226	0.068	89.62
2	5b	2.317	-4.876	411.352	-1.138	168.31	-2.998	0.071	89.67
3	5c	2.798	-4.768	376.133	-0.787	373.182	-2.967	0.168	90.32
4	5d	2.762	-4.789	376.164	-0.767	465.314	-3.012	0.207	90.67
5	5e	2.497	-4.766	318.637	-0.982	154.32	-2.997	0.209	89.13
6	5f	2.231	-4.812	399.258	-0.813	199.87	-2.175	0.098	88.32

^aDihydrorugosaflavonoids; QP log Po/w: predicted octanol/water partition coefficient (acceptable range: -2.0–6.5); QP log HERG: predicted IC₅₀ value for blockage of HERG K⁺ channels (acceptable range: above-5.0); QPP Caco: predicted apparent Caco-2 cell permeability in nm s⁻¹ (Caco-2 cell is a model for the gut–blood barrier) (in nm s⁻¹) (<25, poor; >500, great); QP log BB: predicted brain/blood partition coefficient (-3 to 1.2); QPP MDCK: predicted apparent MDCK cell permeability (in nm s⁻¹) (<25, poor; >500, great) (MDCK cells are considered to be a good mimic for the blood–brain barrier); QP log KP: predicted skin permeability (-8 to -1.0); QP log K_{hsa}: prediction of binding to human serum albumin (acceptable range: -1.5 to 1.5); percentage of human oral absorption (<25% is poor and >80% is high).

-5.0. The values obtained for dihydrorugosaflavonoids were between -4.7 and -4.8, which are above -5.0. QPP Caco gives an idea about the apparent Caco-2 cell permeability in nm s⁻¹. The Caco-2 cell is a model for the gut–blood barrier. Below 25, it is considered as poor, and above 500, it is considered as significantly good. Its computational values for compounds 5a–f were found to be between 318 and 411, which are not great but not poor also. QP log BB calculates the brain–blood partition coefficient. Its acceptable range is -3 to 1.2. The compounds (5a–f) under study showed these values from -1.13 to -0.76. QPP MDCK predicts apparent MDCK cell permeability in nm s⁻¹/MDCK cell, which is identified to be a good imitator for the blood–brain barrier. Its acceptable range is 25–500. Its values for dihydrorugosaflavonoids (5a–f) were obtained between 150 and 465. QP log KP predicts the skin permeability. Its acceptable range is -8 to -1.0. For compounds 5a–f, its values were obtained between -2.9 and -2.1. QP log K_{hsa} predicts affinity toward human serum albumin. Its tolerable limit is -1.5 to 1.5. For compounds 5a–f, its values ranged between 0.68 and 0.207. It is mentioned that the percentage of human oral absorption range of 25% is weak and 80% is significant. For compounds 5a–f, these values were obtained between 88.32 and 90.67. These results support that the compounds have all of the values in the acceptable range.

Antiviral Studies. Cell Cytotoxicity Testing. The tetrazolium-based cell viability assay was conducted to

investigate and detect the maximum nontoxic dose (MNTD) for both the compounds 5c and 5d. The 3-(4,5-dimethylthiazol-2-yl)-2,5-diphenyltetrazolium bromide (MTT) assay is dependent on the reaction of water-soluble compound (MTT) with an insoluble formazan product by viable cells with active metabolic activity. Thus, the color produced due to the formation of formazan is a suitable marker of only viable cells. Different concentrations of the 5c and 5d compounds were assessed by MTT assay at 24 h. Both compounds did not display toxicity up to 85 μM as >70% of Vero cells were viable (Figure 3a,b). Half-maximal cytotoxicity (CC₅₀) was calculated from the plotted graph and represented as a dotted line. So, all of the antiviral assays were performed using 30–70 μM concentration of both the compounds.

Assessment of Antiviral Activity via Cytopathic Effect. After evaluation of MNTD for both the compounds, the different non-cytotoxic concentrations of 5c and 5d compounds were screened on virus-infected Vero cells to find out the possible effects of the compounds. Viral-induced cytopathic effect (CPE) assay was evaluated at 48 hpi (Supporting Information File 1). The compounds 5c and 5d exhibited a significant reduction of CHIKV-induced CPE at less than 70 μM concentration.

Plaque Reduction Assay. The reduction in the CHIKV infectivity in the presence of 5c and 5d compounds was assessed by plaque reduction assay. In the case of 5c compound-treated CHIKV, virus inhibition was observed

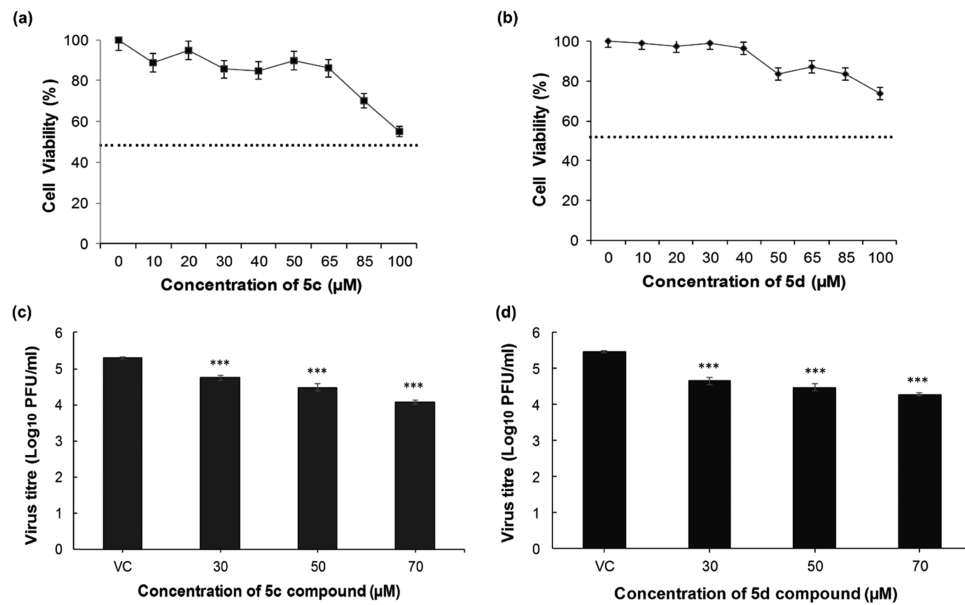


Figure 3. Dihydrorugosaflavonoid cytotoxicity and inhibition assay. (a and b) Cell survival dose-response curves to determine the cytotoxicity of dihydrorugosaflavonoid compounds in Vero cell lines. Compounds' treatment at different concentrations, 10–100 μM , was given to Vero cells for 24 h. (a) **5c**-compound-treated Vero cells; (b) **5d**-compound-treated Vero cells. Percent survival values were obtained based on untreated cells as control. CC_{50} thresholds are marked with a dotted line; (c and d) dose-dependent inhibition of CHIKV shown by **5c** and **5d**, respectively. **5c** and **5d** both exhibit a statistically significant reduction in CHIKV titer at micromolar concentrations. In the analysis, statistical significance is analyzed by the one-way analysis of variance (ANOVA) test and Dunnett's post-test. *** $P < 0.0001$. Values are mean \pm standard deviation of two experiments, which are performed in triplicates. VC is the virus control.

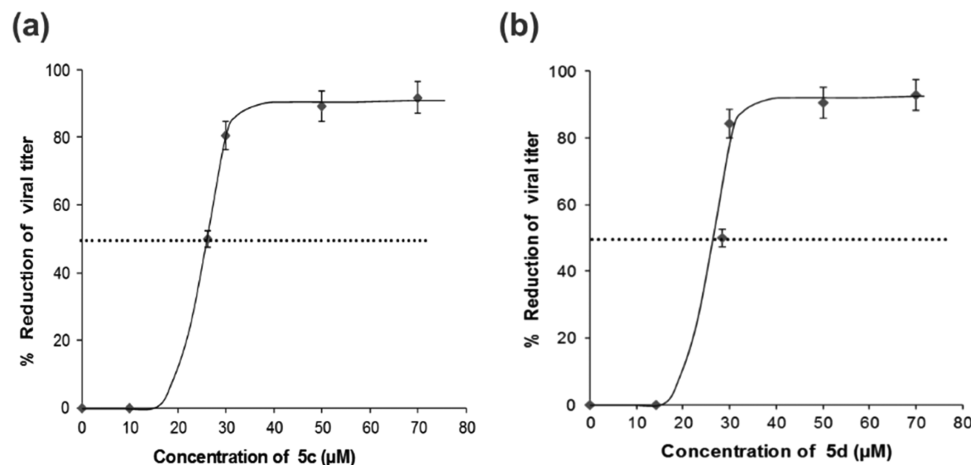


Figure 4. Demonstration of antiviral activity against CHIKV in treated Vero cells. Dihydrorugosaflavonoid-treated Vero cells (pretreated cells) were infected with CHIKV at an MOI of 1 for 90 min. Followed by virus adsorption, the infection medium was changed with the medium containing compounds for 24 h. After 24 hpi, the supernatant was collected for determining percent reduction of viral titer by plaque reduction assay: (a) **5c** compound; (b) **5d** compound. The graphs show the dose-dependent curves of **5c** and **5d**. In the analysis, EC_{50} values of **5c** and **5d** are 26.14 and 28.39 μM , respectively. EC_{50} thresholds are marked with a dotted line. Statistical significance is analyzed by nonlinear regression (curve fit). Values are mean \pm standard deviation of two experiments, which are performed in triplicates.

nearly up to 95% at 70 μM , 88% at 50 μM , and 80% at 30 μM concentration, while **5d**-treated-CHIKV showed 92% at 70 μM , 86% at 50 μM , and 84% at 30 μM , as compared to control (Figure 3). Other compounds (**5a**, **5b**, **5e**, and **5f**) did not show inhibition of CHIKV.

The effective concentration (EC_{50}) of **5c** and **5d** was determined from antiviral curves. The EC_{50} of **5c** compound was 26.14 μM (Figure 4a) with a selectivity index ($\text{CC}_{50}/\text{EC}_{50}$) of 4.33 ($\text{CC}_{50} = 113.4 \mu\text{M}$ (Figure 3a)). The EC_{50} of **5d** compound was 28.39 μM (Figure 4b; selectivity index = 4.19; $\text{CC}_{50} = 119 \mu\text{M}$ (Figure 3b)). The reported EC_{50} values are

the means of two experiments, which are performed in triplicates. It clearly shows that 4'-halogenated dihydrorugosaflavonoids (**5c** and **5d**) possess better inhibitory potential than other substituted dihydrorugosaflavonoid compounds for CHIKV.

Quantitative Real-Time PCR. Conventional RT-PCR methods are still one of the reliable diagnostic methods for studying viral load in supernatants and clinical samples. Here, qRT-PCR was used for validating the antiviral effect of **5c** and **5d** by quantifying CHIKV RNA levels in the infected cells. The reduction in the viral RNA level was observed when treated

with **5c** and **5d** compounds at 24 hpi. The CHIKV RNA levels upon treatment with 70 and 50 μM **5c** were reduced to closely 95 and 90%, respectively, whereas in case of **5d**, with 70 and 50 μM , the RNA levels of CHIKV were reduced to ~93 and 91%, respectively (**Figure 5**).

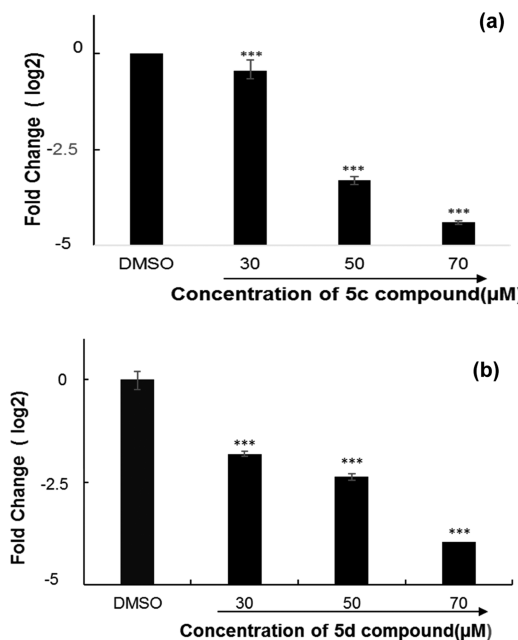


Figure 5. (a, b) Relative quantification of CHIKV mRNA of Vero cells treated with **5c** and **5d** compounds, by real-time PCR. Compounds were added to the cells 12 h before CHIKV infection and were present in the post-infection medium. Viral RNA in infected cells was quantified 24 h post-infection using β -actin as endogenous control by qRT-PCR performed in triplicates. By using the comparative Ct method, the relative amount of mRNA was calculated. The fold change in treated cells was compared with virus control and is presented logarithmically. Statistical significance is analyzed by the one-way ANOVA test and Dunnett's post-test. *** $P < 0.0001$. Values are the mean \pm standard deviation of two experiments, which are performed in triplicates.

Immunofluorescence Assay (IFA). Immunofluorescence staining allows rapid diagnosis of viral antigen in the infected cell using monoclonal antibodies against the virus-specific antigen. One of the two envelope glycoproteins present in the chikungunya virus named E2 glycoprotein has been used as the viral antigen in this study for virus detection by IFA. Here, CHIKV at an MOI of 1 was propagated in Vero cells for 36 h with **5c** and **5d** compounds at 70 and 50 μM concentrations. IFA measured detection of the intracellular virus with an envelope-specific monoclonal antibody (E2 mAb). Additionally, no E2-expression was visualized in a negative control sample, while CHIKV-infected cells were positive for E2-expression. **Figure 6** clearly shows that both **5c** and **5d** compounds inhibited CHIKV at 70 and 50 μM concentrations.

Due to nonavailability of an antiviral drug or vaccine against CHIKV, various approaches have been considered all over the world to identify the lead molecules restricting CHIKV infection or replication. In this piece of work, molecular docking of dihydrorugosaflavonoids with nsP3 showed their interaction with the key residues of nsP3 that bind ADP, which supports the possibility and indicates that these compounds are potential antivirals for CHIKV. This is confirmed in this study

by performing various antiviral assays. The CPE and plaque reduction assay displayed that compounds **5c** and **5d** potentially inhibit CHIKV infection. Further, qRT-PCR assay results clearly show the potential of these two compounds in the suppression of viral RNA levels in infected cells. Furthermore, the antiviral activity of dihydrorugosaflavonoids toward CHIKV is also well delivered by IFA.

CONCLUSIONS

Flavonoid compounds have received many rewards by showing their potential in medicinal chemistry. Dihydrorugosaflavonoids belong to the same class and display their potential to inhibit CHIKV replication. In conclusion, it could be explicated that halogenated dihydrorugosaflavonoids with the appropriate modifications are deserving candidates for additional study to find out the accurate facts of their mechanism of action and effective anti-CHIKV therapeutics.

EXPERIMENTAL SECTION

General Remarks. All of the chemicals utilized during the reactions were obtained from Spectrochem, India. ^1H NMR and ^{13}C NMR spectra were recorded at room temperature on Varian 400 MHz and 100 MHz spectrometers, respectively. Chemical shift values were displayed with reference to TMS as an internal standard. DMSO- d_6 was used as the solvent to prepare the samples. Chemical shifts were expressed in δ (ppm) and coupling constants (J) in Hertz. The splitting pattern abbreviations are as follows: s, singlet; d, doublet; t, triplet; q, quartet; m, unresolved multiplet; dd, doublet of the doublet. Column chromatography was performed with Merck silica gel 60 (230–400 mesh). Analytical thin-layer chromatography was carried out using Merck silica gel 60F₂₅₄, and iodine was used as a developing reagent. IR spectra were recorded on an FTIR IR Affinity-1 Shimadzu spectrophotometer. The CHNS analysis was recorded on Elementar Vario El-III.

Molecular Docking. *Protein Preparation.* Protein (nsP3 PDB code: 3GPO) preparation was performed using Maestro 11.2 software by the protocol in our earlier published paper.³¹ The protein was taken from the RCSB site (www.rcsb.org)

Ligand Preparation. The dihydrorugosaflavonoid derivatives (**5a–f**) were designated as ligands. The ligands were suitably prepared using the Ligprep tool of the same software. The protocol was followed as per the reported procedure.³¹

Receptor Grid Generation. The GLIDE tool was used for the generation of receptor grid in 3GPO. The protocol was followed as per the procedure reported by Puranik et al.³¹

GLIDE Molecular Docking. Molecular docking of 3GPO with dihydrorugosaflavonoids was established with the help of Glide tool. This computation study was carried out as per the protocol reported.³¹

ADME Properties' Calculations. ADME properties of ligand molecules were obtained by the QikProp tool of Schrodinger 2017, which delivered information about absorption, distribution, metabolism, excretion, and toxicity (ADME/T) properties of the ligands. It provided data such as QP log Po/w, QP log BB, overall CNS activity, Caco-2, MDCK cell permeability, $\log K_{hsa}$ for human serum albumin binding, percentage of human oral absorption, etc. The method was conducted as per the protocol published.³¹

Chemistry. All of the compounds **5a–f** and their intermediates were synthesized as per the procedure reported

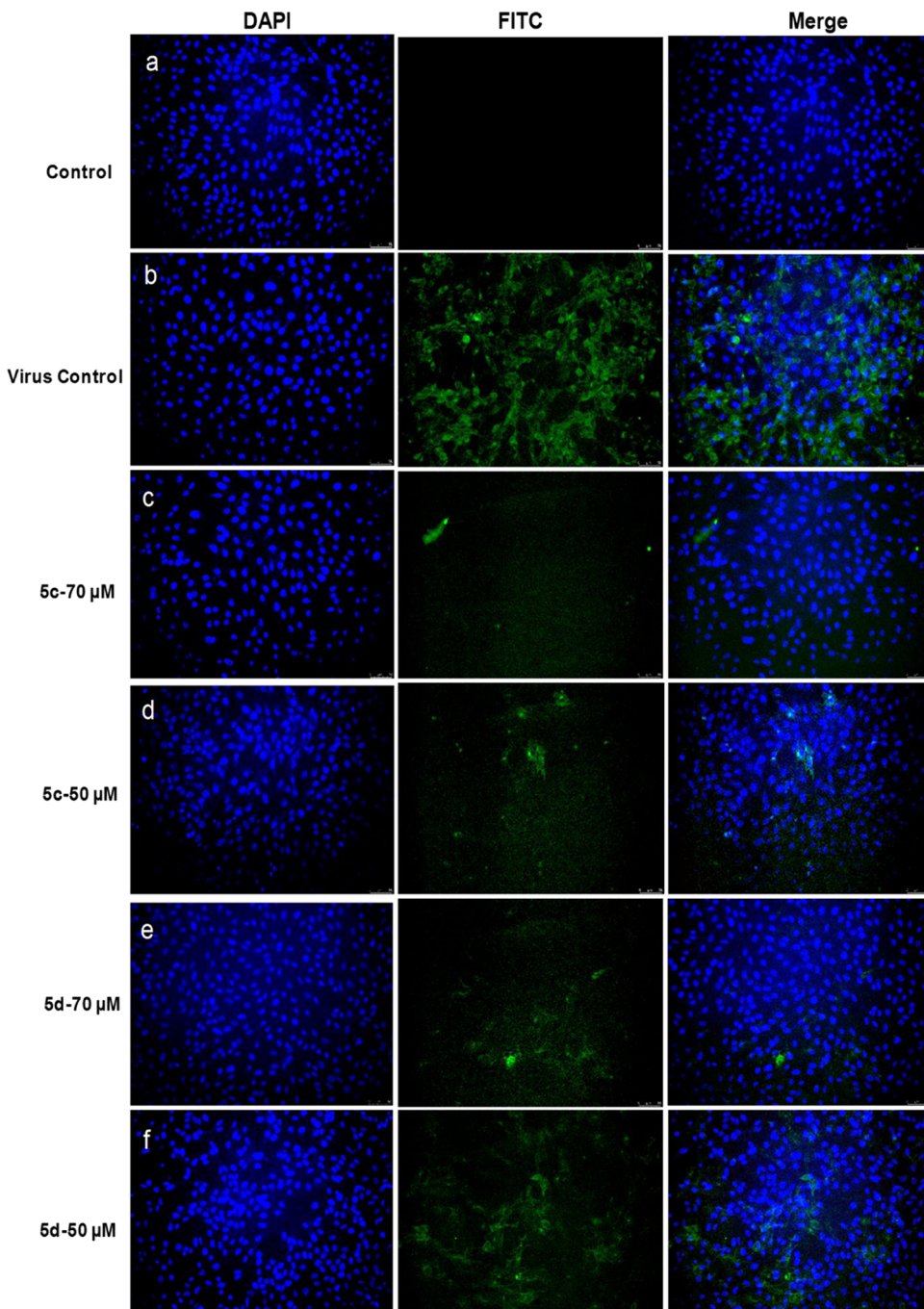


Figure 6. Evaluation of the antiviral effect by indirect immunofluorescence assay (IFA). Viral inhibition was assessed by IFA by treatment with **5c** and **5d** compounds. Cells were observed at 36 hpi; micrographs with green fluorescence indicate the virus load as determined with anti-E2 mAb and fluorescein isothiocyanate (FITC) conjugated secondary antibody (green), and blue fluorescence indicates the nuclear staining with 4',6-diamidino-2-phenylindole (DAPI). Infected Vero cells with compound treatment (**5c**, 70 μ M (c); **5c**, 50 μ M (d); **5d**, 70 μ M (e); **5d**, 50 μ M (f)) and cell control (containing no virus (a)) are shown. Virus control images are represented in (b). Cells were observed by a fluorescent microscope (Leica Microsystems) with a 20 \times objective lens. Scale bar is 50 μ m.

in our previous published paper.³¹ The details are provided in Supporting Information File 1.

Antiviral Cell-Based Assays. Cells and Viruses. Vero cells (NCCS, Pune, India) were maintained in Dulbecco's modified Eagle's medium (DMEM; HiMedia, India) supplemented with 10% heat-inactivated fetal bovine serum (FBS; Gibco), 100 units of penicillin, and 100 mg of streptomycin/mL at 37 °C and in a 5% CO₂ incubator. Using the virus adsorption technique, CHIKV (accession number, KY057363.1; strain,

119067)⁵⁰ stocks were prepared in Vero cells and stored at -80 °C until needed. By using the plaque-forming assay, the virus titer is calculated. Plaque-forming unit per milliliter (PFU/mL) was used to quantify the virus titer.

Cytotoxicity Studies. The cytotoxicity of **5c** and **5d** compounds for Vero cells was measured using MTT (Sigma) in a 96-well plate format. Stocks of **5c** and **5d** compounds were prepared by dissolving in dimethyl sulfoxide (DMSO), and the working concentration was prepared by

further diluting in culture media. At 90% confluence, the media were removed, and media containing different dilutions of compounds were added into each well. Wells with 0.1% DMSO were considered as control. After 24 h, MTT was added to each 96-well in a volume of 20 μ L of 5 mg mL⁻¹ stock and incubated for 4 h at 37 °C in 5% CO₂. Upon completion of incubation, DMSO was added to dissolve formazan crystals. The absorbance was read at a wavelength of 570 nm using a multi-mode plate reader (BioTek Instruments, Inc.). The experiment was done in triplicates.

Assessment of Antiviral Activity. Vero cells were seeded onto a 24-well plate at a cell density of 2×10^5 cells/well. Cells were treated with compounds 12 h prior to infection (before infection). At MOI of 1, the cell monolayer was infected with CHIKV with gentle shaking after every 15 min for 90 min. The inoculum was discarded, and the cell monolayer was washed twice to ensure that there is no chance of secondary infection. Compounds were also added in the post-infection media containing DMEM with 2% FBS for 24 h (after infection). Infected cells were incubated with 0.1% DMSO as the negative control. After 24 hpi, the supernatant was collected for determining virus titer by plaque-forming assay. After collecting the supernatant, TRIzol (Thermo Fisher Scientific) was added (as per manufacturer's protocol) to the adherent cells in a 24-well plate to isolate RNA for qRT-PCR. Furthermore, the CPE of CHIKV on the Vero cell line appeared in ~48 h after the cell infection. Hence, the effect of inhibitory compounds on the CPE was observed after 48 hpi with an inverted light microscope (Carl Zeiss, Germany). Dose-response cell viability and antiviral curves were used to determine EC₅₀ and CC₅₀. The ratio of CC₅₀/EC₅₀ is the selectivity index, which gave an idea of the therapeutic window of the dihydrorugosaflavonoid compounds.

Plaque Reduction Assay. To perform the plaque assay for measuring the virus titer, a Vero cell monolayer was seeded in 24-well plates at 2×10^5 cells per well. **5c** and **5d** compound treatment and infection were the same as described in the assessment of antiviral activity. The final DMSO concentration in both the compounds was 0.01% v/v. The infected cells were treated with varying concentrations of each compound in DMEM with 2% FBS and incubated at 37 °C and 5% CO₂ for 24 h. At 24 hpi, the cell supernatant was harvested, and the 10-fold serial-diluted CHIKV supernatant was added to the Vero cells and incubated at 37 °C for 90 min while the untreated but virus-infected cells were taken as control. Afterward, cells were overlaid with 1% carboxymethyl cellulose in MEM with 2% FBS and incubated at 37 °C and 5% CO₂. After 48 h, the overlay medium was discarded, then the cells were fixed with 10% formaldehyde for 2 h, and cells were stained with 1% crystal violet solution for plaque visualization.

Dose-response curves were generated by measuring percent inhibition in the plaque reduction assay for a particular range of compound concentrations. Varying concentrations of each compound were used to generate inhibition curves for calculating the 50% effective concentration (EC₅₀). EC₅₀ of each compound was calculated by plotting the graph of percent inhibition of the compound at different concentrations vs. compound concentration. The plaque reduction assay was performed in triplicates for a particular concentration of the compound and was repeated twice to verify the constant inhibition results.

Quantitative Real-Time (qRT) PCR. Vero cells were seeded onto 12-well plates at a cell density of 4×10^5 cells per

well.^{16,17} **5c** and **5d** compounds' treatment and infection were the same as described in the assessment of antiviral activity. For quantification of viral genome after 24 h of incubation with or without the compound, the supernatant was discarded and trizol was added to the plate. RNA was purified according to the manufacturer's protocol. Purified RNA was treated with DNase to remove any traces of genomic DNA (Promega) and then subsequently used for cDNA preparation using the AccuScript high fidelity cDNA synthesis kit (Agilent) with 1 μ g of extracted RNA. The forward and reverse primers used for amplification^{51,52} are given in Table 4.

Table 4. Sequence of Oligonucleotides Used as Primers in CHIKV Virus in Quantitative Real-Time Polymerase Chain Reaction (qRT-PCR)

primers	5'-3' sequence	length (base pair)
E1 forward primer	AAGTACACTGTGCAGCTGAGT	21
E1 reverse primer	GCATAGCACCACGATTAGAATC	22
β -actin forward primer	ATTGCCGACAGGGATGCAGAA	20
β -actin reverse primer	GCTGATCCACATCTGCTGGAA	21

Negative and positive controls were included for PCR amplification. Nuclease-free water was used instead of the RNA sample as a negative control to screen possible contamination. RNA extracted from the untreated CHIKV supernatant was used as a positive control. Experiments were done in triplicate and repeated twice for accuracy of the result. PCR runs were carried out according to the standard KAPA SYBR fast universal qPCR kit on a QuantStudio 5 System (Applied Biosystems, Carlsbad, CA). The cycling conditions are as follows: 95 °C for 20 s and then 40 cycles of 95 °C for 1 s and 60 °C for 20 s. Fluorescence was detected after each cycle. To analyze data, fold change difference between control samples and compound-treated samples was calculated using $\Delta\Delta Ct$ values.

Immunofluorescence Assay. Vero cells were seeded onto a 6-well plate at a cell density of 1×10^6 cells per well. Cells were treated with 70 and 50 μ M concentrations of **5c** and **5d** compounds prior to and after CHIKV infection. At 36 hpi, cells were washed three times with PBS and then fixed with methanol:acetone (1:1) for 1 h at room temperature followed by permeabilization with 0.1% Triton-X-100. After washing, cells were incubated with antibodies against CHIKV, i.e., anti-alphavirus (1:100, SANTA Cruz Biotechnology, Inc.), for 1 h and then incubated with fluorescein (FITC)-conjugated secondary anti-mouse antibody (1:250, Sigma) for 30 min at 37 °C. The plate was then rinsed with PBS and counter-stained with DAPI (Sigma) for 15 min. Then, the image was captured by two trained persons, under a fluorescence microscope (Leica Microsystems). All experiments were repeated thrice to verify the results.

ASSOCIATED CONTENT

S Supporting Information

The Supporting Information is available free of charge on the ACS Publications website at DOI: [10.1021/acsomega.9b02900](https://doi.org/10.1021/acsomega.9b02900).

(1) Image of cytopathic effect and (2) spectra of all of the compounds **5a–f**; (3) detailed protocol for the

molecular modeling, ADME study, and procedure for the synthesis of **5a–f** (PDF)

AUTHOR INFORMATION

Corresponding Authors

*E-mail: shaifbt@iitr.ac.in (S.T.).

*E-mail: psrivastava@aripune.org (P.S.).

ORCID

Pratibha Srivastava: [0000-0002-4562-2773](https://orcid.org/0000-0002-4562-2773)

Author Contributions

†N.V.P. and R.R. have equal contribution in this piece of work.

Notes

The authors declare no competing financial interest.

ACKNOWLEDGMENTS

N.V.P. is thankful to Agharkar Research Institute, Pune, for financial support. S.T. acknowledges the financial support from the Indian Council of Medical Research (ICMR: Ref no. BIC/12(26)/2013).

REFERENCES

- (1) Abdelnabi, R.; Neyts, J.; Delang, L. Chikungunya virus infections: time to act, time to treat. *Curr. Opin. Virol.* **2017**, *24*, 25–30.
- (2) Morrison, T. E. Reemergence of chikungunya virus. *J. Virol.* **2014**, *88*, 11644–11647.
- (3) National Vector Borne Disease Control Programme. Chikungunya Fever. <http://nvbdcp.gov.in/chikun-status.html> (accessed April 2018).
- (4) Choi, H. K.; Lee, S.; Zhang, Y. P.; McKinney, B. R.; Wengler, G.; Rossmann, M. G.; Kuhn, R. J. Structural analysis of Sindbis virus capsid mutants involving assembly and catalysis. *J. Mol. Biol.* **1996**, *262*, 151–167.
- (5) Lee, S.; Owen, K. E.; Choi, H. K.; Lee, H.; Lu, G.; Wengler, G.; Brown, D. T.; Rossmann, M. G.; Kuhn, R. J. Identification of a protein binding site on the surface of the alphavirus nucleocapsid and its implication in virus assembly. *Structure* **1996**, *4*, 531–541.
- (6) Mancini, E. J.; Clarke, M.; Gowen, B. E.; Rutten, T.; Fuller, S. D. Cryo-electron microscopy reveals the functional organization of an enveloped virus, Semliki Forest virus. *Mol. Cell* **2000**, *5*, 255–266.
- (7) Zhang, W.; Mukhopadhyay, S.; Pletnev, S. V.; Baker, T. S.; Kuhn, R. J.; Rossmann, M. G. Placement of the structural proteins in Sindbis virus. *J. Virol.* **2002**, *76*, 11645–11658.
- (8) Mukhopadhyay, S.; Zhang, W.; Gabler, S.; Chipman, P. R.; Strauss, E. G.; Strauss, J. H.; Baker, T. S.; Kuhn, R. J.; Rossmann, M. G. Mapping the structure and function of the E1 and E2 glycoproteins in alphaviruses. *Structure* **2006**, *14*, 63–73.
- (9) Voss, J. E.; Vaney, M. C.; Duquerroy, S.; Vonrhein, C.; Girard-Blanc, C.; Crublet, E.; Thompson, A.; Bricogne, G.; Rey, F. A. Glycoprotein organization of Chikungunya virus particles revealed by X-ray crystallography. *Nature* **2010**, *468*, 709–712.
- (10) Sherman, M. B.; Weaver, S. C. Structure of the recombinant alphavirus western equine encephalitis virus revealed by cryoelectron microscopy. *J. Virol.* **2010**, *84*, 9775–9782.
- (11) Kostyuchenko, V. A.; Jakana, J.; Liu, X.; Haddow, A. D.; Aung, M.; Weaver, S. C.; Chiu, W.; Lok, S. M. The structure of barmah forest virus as revealed by cryo-electron microscopy at a 6-angstrom resolution has detailed transmembrane protein architecture and interactions. *J. Virol.* **2011**, *85*, 9327–9333.
- (12) Long, F.; Fong, R. H.; Austin, S. K.; Chen, Z.; Klose, T.; Fokine, A.; Liu, Y.; Porta, J.; Sapparapu, G.; Akahata, W.; Doranz, B. J. Cryo-EM structures elucidate neutralizing mechanisms of anti-chikungunya human monoclonal antibodies with therapeutic activity. *Proc. Natl. Acad. Sci. U.S.A.* **2015**, *112*, 13898–13903.
- (13) Vasiljeva, L.; Merits, A.; Auvinen, P.; Kääriäinen, L. Identification of a novel function of the alphavirus capping apparatus RNA 5'-Triphosphatase activity of Nsp2. *J. Biol. Chem.* **2000**, *275*, 17281–17287.
- (14) Soonsawad, P.; Xing, L.; Milla, E.; Espinoza, J. M.; Kawano, M.; Marko, M.; Hsieh, C.; Furukawa, H.; Kawasaki, M.; Weerachayanukul, W. Structural evidence of glycoprotein assembly in cellular membrane compartments prior to Alphavirus budding. *J. Virol.* **2010**, *84*, 11145–11151.
- (15) Shirako, Y.; Strauss, E. G.; Strauss, J. H. Suppressor mutations that allow Sindbis virus RNA polymerase to function with nonaromatic amino acids at the N-terminus: evidence for interaction between nsP1 and nsP4 in minus-strand RNA synthesis. *Virology* **2000**, *276*, 148–160.
- (16) Sharma, R.; Kesari, P.; Kumar, P.; Tomar, S. Structure function insights into chikungunya virus capsid protein: Small molecules targeting capsid hydrophobic pocket. *Virology* **2018**, *515*, 223–234.
- (17) Tomar, S.; Narwal, M.; Harms, E.; Smith, J. L.; Kuhn, R. J. Heterologous production, purification and characterization of enzymatically active Sindbis virus nonstructural protein nsP1. *Protein Expr. Purif.* **2011**, *79*, 277–284.
- (18) McPherson, R. L.; Abraham, R.; Sreekumar, E.; Ong, S. E.; Chenga, S. J.; Baxter, V. K.; Kistemakere, H. A.; Filippov, D. V.; Griffin, D. E.; Leung, A. K. ADP-ribosylhydrolase activity of Chikungunya virus macrodomain is critical for virus replication and virulence. *Proc. Natl. Acad. Sci. U.S.A.* **2017**, *114*, 1666–1671.
- (19) Kam, Y. W.; Ong, E. K.; Renia, L.; Tong, J. C.; Ng, L. F. Immuno-biology of Chikungunya and implications for disease intervention. *Microbes. Infect.* **2009**, *11*, 1186–1196.
- (20) McClain, D. J.; Pittman, P. R.; Ramsburg, H. H.; Nelson, G. O.; Rossi, C. A. Immunologic interference from sequential administration of live attenuated alphavirus vaccines. *J. Infect. Dis.* **1998**, *177*, 634–641.
- (21) Briolant, S.; Garin, D.; Scaramozzino, N.; Jouan, A.; Crance, J. M. In vitro inhibition of Chikungunya and Semliki Forest viruses replication by antiviral compounds: synergistic effect of interferon-alpha and ribavirin combination. *Antiviral Res.* **2004**, *61*, 111–117.
- (22) Delogu, I.; de Lamballerie, X. Chikungunya disease and chloroquine treatment. *J. Med. Virol.* **2011**, *83*, 1058–1059.
- (23) Delogu, I.; Pastorino, B.; Baronti, C.; Nougairede, A.; Bonnet, E. In vitro antiviral activity of arbidol against Chikungunya virus and characteristics of a selected resistant mutant. *Antiviral Res.* **2011**, *90*, 99–107.
- (24) Ravichandran, R.; Manian, M. Ribavirin therapy for Chikungunya arthritis. *J. Infect. Dev. Ctries.* **2008**, *2*, 140–142.
- (25) Pohjala, L.; Utt, A.; Varjak, M.; Lulla, A.; Merits, A. Inhibitors of alphavirus entry and replication identified with a stable Chikungunya replicon cell line and virus-based assays. *PLoS One* **2011**, *6*, No. e28923.
- (26) Lucas-Hourani, M.; Lupon, A.; Despres, P.; Thoret, S.; Pamlard, O. A phenotypic assay to identify Chikungunya virus inhibitors targeting the nonstructural protein nsP2. *J. Biomol. Screen.* **2013**, *18*, 172–179.
- (27) Gaspar, A.; Matos, M. J.; Garrido, J.; Uriarte, A.; Borges, F. Chromone: A valid scaffold in medicinal chemistry. *Chem. Rev.* **2014**, *114*, 4960–4992.
- (28) Kozlowska, A.; Szostak-Węgierska, D. Flavonoids—Food Sources, Health Benefits, and Mechanisms Involved. In *Bioactive Molecules in Food*; Mérillon, J. M., Ramawat, K., Eds.; Reference Series in Phytochemistry; Springer: Cham, 2018; pp 1–27.
- (29) Hu, Q. F.; Zhou, B.; Huang, J. M.; Jiang, Z. Y.; Huang, X. Z.; Yang, L. Y.; Gao, X. M.; Yang, G. Y.; Che, C. T. Cytotoxic oxeepinochromone and flavonoids from the flower buds of Rosa rugosa. *J. Nat. Prod.* **2013**, *76*, 1866–1871.
- (30) Puranik, N. V.; Srivastava, P. First synthesis of rugosaflavonoid and its derivatives and their activity against breast cancer. *RSC Adv.* **2017**, *7*, 33052–33060.
- (31) Puranik, N. V.; Srivastava, P.; Swami, S.; Choudhari, A.; Sarkar, D. Molecular modeling studies and in-vitro screening of dihydrorugosaflavonoids and its derivatives against Mycobacterium tuberculosis. *RSC Adv.* **2018**, *8*, 10634–10643.

- (32) Cruz, D. J. M.; Bonotto, R. M.; Gomes, R. G. B.; DaSilva, C. T.; Taniguchi, J. B.; Hwan No, J. H.; Lombardot, B.; Schwartz, O.; Hansen, M. A. E.; Freitas-Junior, L. H. Identification of Novel Compounds Inhibiting Chikungunya Virus-Induced Cell Death by High Throughput Screening of a Kinase Inhibitor Library. *PLoS Negl. Trop. Dis.* **2013**, *7*, No. e2471.
- (33) Eckei, L.; Krieg, S.; Bütepage, M.; Lehmann, A.; Gross, A.; Lippok, B.; Grimm, A. R.; Beate, M.; Kümmeler, B. M.; Rossetti, G.; Lüscher, B.; Verheggen, P. The conserved macrodomains of the non-structural proteins of Chikungunya virus and other pathogenic positive strand RNA viruses function as mono-ADP ribosylhydrolases. *Sci. Rep.* **2017**, *7*, No. 41746.
- (34) Lani, R.; Hassandarvish, P.; Wai; Shu, M. H.; Wai, H. P.; Chu, J. J. H.; Higgs, S.; Vanlandingham, D.; Bakar, S. A.; Zandi, K. Antiviral activity of selected flavonoids against Chikungunya virus. *Antiviral Res.* **2016**, *133*, 50–61.
- (35) Fros, J. J.; Domeradzka, N. E.; Baggen, J.; Geertsema, C.; Flipse, J.; Vlak, J. M.; Pijlman, G. P. Chikungunya virus nsP3 blocks stress granule assembly by recruitment of G3BP into cytoplasmic foci. *J. Virol.* **2012**, *86*, 10873–10879.
- (36) Thaa, B.; Biasiotto, R.; Eng, K.; Neuvonen, M.; Götte, B.; Rheinemann, L.; Mutso, M.; Utt, A.; Varghese, F.; Balistreri, G.; Merits, A.; Ahola, T.; McInerney, G. M. Differential PI3K-Akt-mTOR activation by Semliki Forest and chikungunya virus, dependent on nsP3 and connected to replication complex internalisation. *J. Virol.* **2015**, *89*, 11420–11437.
- (37) Neuvonen, M.; Kazlauskas, A.; Martikainen, M.; Hinkkanen, A.; Ahola, T.; Saksela, K. SH3 domain-mediated recruitment of host cell amphiphysins by alphavirus nsP3 promotes viral RNA replication. *PLoS Pathog.* **2011**, *7*, No. e1002383.
- (38) Park, E.; Griffin, D. E. Interaction of Sindbis virus non-structural protein 3 with poly (ADP-ribose) polymerase 1 in neuronal cells. *J. Gen. Virol.* **2009**, *90*, 2073–2080.
- (39) Gorbalyena, A. E.; Koonin, E. V.; Lai, M. M. Putative papain-related thiol proteases of positive-strand RNA viruses. Identification of rubi- and aphthovirus proteases and delineation of a novel conserved domain associated with proteases of rubi-, alpha and coronaviruses. *FEBS Lett.* **1991**, *288*, 201–205.
- (40) Koonin, E. V.; Gorbalyena, A. E.; Purdy, M. A.; Rozanov, M. N.; Reyes, G. R.; Bradley, D. W. Computer-assisted assignment of functional domains in the nonstructural polyprotein of hepatitis E virus: delineation of an additional group of positive-strand RNA plant and animal viruses. *Proc. Natl. Acad. Sci. U.S.A.* **1992**, *89*, 8259–8263.
- (41) Rack, J. G. M.; Perina, D.; Ahel, I. Macrodomains: Structure, function, evolution, and catalytic activities. *Annu. Rev. Biochem.* **2016**, *85*, 431–454.
- (42) Eriksson, K. K.; Cervantes-Barragán, L.; Ludewig, B.; Thiel, V. Mouse hepatitis virus liver pathology is dependent on ADP-ribose-1'-phosphatase, a viral function conserved in the alpha-like supergroup. *J. Virol.* **2008**, *82*, 12325–12334.
- (43) Fehr, A. R.; Athmer, J.; Channappanavar, R.; Phillips, J. M.; Meyerholz, D. K.; Perlman, S. The nsP3 macrodomain promotes virulence in mice with coronavirus induced encephalitis. *J. Virol.* **2015**, *89*, 1523–1536.
- (44) Putics, A.; Filipowicz, W.; Hall, J.; Gorbalyena, A. E.; Ziebuhr, J. ADP-ribose-1'-monophosphatase: A conserved coronavirus enzyme that is dispensable for viral replication in tissue culture. *J. Virol.* **2005**, *79*, 12721–12731.
- (45) Kuri, T.; Eriksson, K. K.; Putics, A.; Züst, R.; Snijder, E. J.; Davidson, A. D.; Siddell, S. G.; Thiel, V.; Ziebuhr, J.; Weber, F. The ADP-ribose-1'-monophosphatase domains of severe acute respiratory syndrome coronavirus and human coronavirus 229E mediate resistance to antiviral interferon responses. *J. Gen. Virol.* **2011**, *92*, 1899–1905.
- (46) Fehr, A. R.; Channappanavar, R.; Jankevicius, G.; Fett, C.; Zhao, J.; Athmer, J.; Meyerholz, D. K.; Ahel, I.; Perlman, S. The conserved coronavirus macrodomain promotes virulence and suppresses the innate immune response during severe acute respiratory syndrome coronavirus infection. *mBio* **2016**, *7*, No. e01721-16.
- (47) Rungrotmongkol, T.; Nunthaboot, N.; Malaisreea, M.; Kaiyawet, N.; Yotmanee, P.; Meeprasert, A.; Hannongbua, S. Molecular insight into the specific binding of ADP-ribose to the nsP3 macro domains of chikungunya and venezuelan equine encephalitis viruses: Molecular dynamics simulations and free energy calculations. *J. Mol. Graph. Model.* **2010**, *29*, 347–353.
- (48) Krüger, A.; Maltarollo, V. G.; Wrenger, C.; Kronenberger, T. ADME Profiling in Drug Discovery and a New Path Paved on Silica. In *Drug Discovery and Development- New Advances*; Intech Open Publishers, 2019; pp 1–31.
- (49) Hodgson, J. ADMET—Turning chemicals into drugs. *Nat. Biotechnol.* **2001**, *19*, 722–726.
- (50) Singh, H.; Mudgal, R.; Narwal, M.; Kaur, R.; Singh, V. S.; Malik, A.; Chaudhary, M.; Tomar, S. Chikungunya virus inhibition by peptidomimetic inhibitors targeting virus-specific cysteine protease. *Biochimie* **2018**, *149*, 51–61.
- (51) Kaur, R.; Mudgal, R.; Jose, J.; Kumar, P.; Tomar, S. Glycan-dependent chikungunya viral infection divulged by antiviral activity of NAG specific chi-like lectin. *Virology* **2019**, *526*, 91–98.
- (52) Seyed, S. S.; Munirah Shukri, M.; Pouya Hassandarvish, P.; Adrian Oo, A.; Muthu, S. E.; Abubakar, S.; Zandi, K. Computational Approach Towards Exploring Potential Anti-Chikungunya Activity of Selected Flavonoids. *Sci. Rep.* **2016**, *6*, No. 24027.